Ensemble Joint Sparse Low-Rank Matrix Decomposition for Thermography Diagnosis System

Junaid Ahmed [ID], Bin Gao [ID], *Senior Member, IEEE*, Wai Lok Woo [ID], *Senior Member, IEEE*, and Yuyu Zhu

Abstract—**Composite is widely used in the aircraft industry and it is essential for manufacturers to monitor its health and quality. The most commonly found defects of composite are debonds and delamination. Different inner defects with complex irregular shape are difficult to diagnosed by using conventional thermal imaging methods. In this article, an ensemble joint sparse low-rank matrix decomposition algorithm is proposed by applying the optical pulse thermography (OPT) diagnosis system. The proposed algorithm jointly models the low-rank and sparse pattern by using concatenated feature space. In particular, the weak defects information can be separated from strong noise and the resolution contrast of the defects has significantly been improved. Ensemble iterative sparse modeling are conducted to further enhance the weak information as well as reducing the computational cost. In order to show the robustness and efficacy of the model, experiments are conducted to detect the inner debond on multiple carbon fiber reinforced polymer composites. A comparative analysis is presented with general OPT algorithms. Notwithstanding above, the proposed model has been evaluated on synthetic data and compared with other low-rank and sparse matrix decomposition algorithms.**

Index Terms—**Carbon fiber reinforced polymer (CFRP) composites, concatenated matrix factorization, eigendecomposition, low-rank sparse decomposition, optical thermography, weak signal detection.**

I. INTRODUCTION

THE USAGE of carbon fiber reinforced polymer (CFRP) in the aerospace and aircraft industry is increasing, largely

Junaid Ahmed, Bin Gao, and Yuyu Zhu are with the School of Automation Engineering, University of Electronic Science and Technology, Chengdu 610054, China (e-mail: junaid_ahmedtl@hotmail.com; bin_gao@uestc.edu.cn; yuyuzhu@uestc.edu.cn).

Wai Lok Woo is with the Department of Computer and Information Sciences, Faculty of Engineering and Environment, Northumbria University, Newcastle upon Tyne NE1 8ST, U.K. (e-mail: wailok.woo@northumbria.ac.uk).

Color versions of one or more of the figures in this article are available online at http://ieeexplore.ieee.org.

owing to its unique characteristics as lightweight, stiffness, and resistance to corrosion. For quality assurance to monitor the health and quality of the composite becomes ever more important [1]. The composites are manufactured by sandwiching different layers. For good quality, the layers should have strong bonding. However, due to the manufacturing limitations and installation procedure, defects become inevitable. The most commonly found defects in the composites are debonds and delaminations [2]. These defects occur on the inner part of the composite and are not easily detected. Therefore, nondestructive testing (NDT) and structural health monitoring are necessary.

Poudel *et al.* [3] used the NDT technique for defect detection and analysis of composite repairs. Meola *et al.* [4] reviewed the importance of NDT-based methods for defect analysis in the composites. The NDT techniques usually use different external sources for defect analysis. Based on this principle, the NDT can be categorized as eddy current based NDT [5], ultrasonic-based NDT [6], acoustic emission-based NDT [7], and microwave-based NDT [8]. Nowadays, the popular NDT method for composite defect detection is the optical pulse thermography (OPT) [9]–[12]. It is a fast and wide-area inspection technique and more detailed review of OPT system can be found in [13] and [14].

Maierhofer *et al.* [2] discussed two modes of OPT, i.e., reflection and transmission modes. A more detailed description of the type and usage of the excitation sources for the OPT can be found in [15] and [16]. The OPT uses an excitation source to induce temperature variation in the composite. If defects exist, irregular patterns occur and are captured by the infrared camera. These thermal frames in raw form contain a large degree of noise while the information on defects is not clear. To improve the contrast of defects and remove noise, the image and video processing algorithms are utilized [17]–[21].

The generally used image pattern analysis technique for defect detection by an OPT system is the principal component analysis (PCA) [22]–[24]. It is based on low-rank estimation using singular value decomposition (SVD). In [25], an independent component analysis algorithm is proposed to further enhance the thermal contrast. In [26], a thermal signal reconstruction (TSR) algorithm is proposed. It works on polynomial fitting in the logarithmic domain. In [27] and [28], a pulse phase thermography (PPT) algorithm is proposed for defect detection by analyzing the information on the defects in the frequency domain. Yuanlin *et al.* [29] proposed a novel polynomial fitting coefficient algorithm. It is based on the mixture of fitting time

derivative and the coefficient algorithm. Yousefi *et al.* [30] proposed a candid covariance-free incremental principal component thermography algorithm. The algorithm is an extension to the PCA by decreasing its computational load and increasing the performance. López *et al.* [31] evaluated the performance of the TSR algorithm against the partial least square thermography (PLST) technique. The comparison is carried out for CFRP composite debond detection. Junyan *et al.* [32] proposed a hybrid algorithm based on the simulation annealing and Nelder–Mead simplex search. Zhang *et al.* [33] proposed an algorithm for feature embedding. The algorithm utilizes the concatenated feature space to perform the low-rank sparse matrix approximation. Ishikawa *et al.* [34] proposed an extension to the PPT algorithm. They use phase difference between the defect and nondefect regions at the high frequencies for defect quantification. The research works in [35] and [36] proposed a novel sparse principal component thermography (SPCT) algorithm based on the PCA [22] for defect detection in CFRP composites using optical thermography. The algorithm [35] is quite simple and robust for flat-shaped CFRP specimens. However, it is not validated for complex and irregular shape CFRP specimens as well as the varying depths. From the aspect of low-rank matrix factorization (LRMF), the algorithm [35] is a two-term decomposition algorithm. However, the proposed algorithm optimizes the low-rank and sparse data jointly in a concatenated feature space in a tridecomposition framework. The proposed algorithm is tested for different specimens with different shapes as well as varying depth for a CFRP specimen. In addition, the proposed algorithm is validated on synthetic data with comparison of other low-rank sparse matrix decomposition algorithms. In [37], it presented and compared three different matrix factorization algorithms for defect detection using thermal NDT. The three algorithms include PCA, nonnegative matrix factorization, and archetypal analysis. All methods are tested on thermographic NDT data and analysis is presented. Yousefi *et al.* [38] further tested more algorithms on the thermal NDT data. Moreover, wider applications of the thermal NDT are described such as arts, archeology, and civil structures. The matrix decomposition algorithms are evaluated for these applications and results are analyzed. Feng *et al.* [39] proposed a hybrid algorithm based on the TSR and region growing technique for the task of debond detection in the CFRP composites. Peng *et al.* [40] proposed a multilayer architecture utilizing the ensemble variation based tensor factorization (EVBTF). The algorithm is tested for debond detection in CFRP composites. Ahmed *et al.* [41] proposed a sparse-mixture-of-Gaussian (S-MOG) algorithm for debond detection in CFRP composites. The algorithm utilizes the multilayer structure to mine the features for thermographic image enhancement.

The proposed algorithm falls into the category of tridecomposition-based algorithms. Zhou *et al.* [42] proposed a three-term decomposition model called stable principal component pursuit. In this model, the noise term is modeled to be independent identically distributed. The model is solved iteratively by solving the sparse term with a difference equation and the low-rank term is estimated by using the least square method. Aravkin *et al.* [43] proposed variation of the stable principal component pursuit method. In this model, it decomposes the matrix into the two parts as they are solved sequentially by projected and accelerated gradient methods. Oreifej *et al.* [44] proposed a novel model for the background and foreground segmentation problem in video sequences. They solve the three-term decomposition model in an iterative manner in the framework of the augmented Lagrangian multiplier method. Zhang *et al.* [45] proposed a tridecomposition model in the framework of low-rank matrix recovery and completion. It decomposes the observed data into the clean data, sparse data, and noise data. It is tested in a variety of face images and surveillance videos in the framework of image denoising. These algorithms utilize a single feature space for the optimization of the tridecomposition model containing the observed raw data using the augmented Lagrangian multiplier method. The proposed method utilizes the concatenated feature space for the low-rank matrix decomposition using the residual and sparse data along with the observed raw data. The low-rank information from the concatenated feature space is able to extract the weak target defect information as the defects information lies in the low rank as well as sparse space. In addition, the proposed method solves the tridecomposition model by developing an expectation–maximization (EM) framework for the ensemble joint sparse low-rank matrix decomposition (EJSLRMD).

As the defects depth increases, the detection performance decay. For the composite specimen with an irregular shape, the general OPT algorithms give poor performance [41]. The algorithm given in [41] has good reasonable results, whereas its computational cost is quite high due to the multilayer sparse modeling structure. To alleviate this problem, we propose an EJSLRMD algorithm. The proposed algorithm models the low-rank and sparse data jointly in a concatenated feature space. Since the defects information mostly presents in the sparse and low-rank space, it is possible to mine the low-rank feature in a concatenated feature space with the raw data before sparse modeling. To reduce the computational cost, we chose the most significant eigenfeatures for the sparse modeling. The proposed algorithm is able to detect weaker and deeper defects. In order to show its efficacy, the algorithm is conducted for debond defects detection in a different structure of CFRP composites. The visual analysis along with *F*-score [40] comparison is presented with generally used OPTNDT algorithms. In addition, the proposed algorithm is validated on the synthetic data with different noise configurations.

The rest of this article is organized as follows. Section II describes the proposed algorithm Section III gives the experimental setup and information about the CFRP specimen. Section IV elaborates on the results and discussions. Finally, Section V concludes this article.

II. PROPOSED METHODOLOGY

A. Proposed Algorithm

Given the data tensor containing the thermographic sequences $D \in \mathbf{R}^{m \times n \times k}$ where (m, n) denote the spatial resolution of the frame and k represents the number of the frame. First, we convert it into a matrix form by representing each (m, n) spatial frame
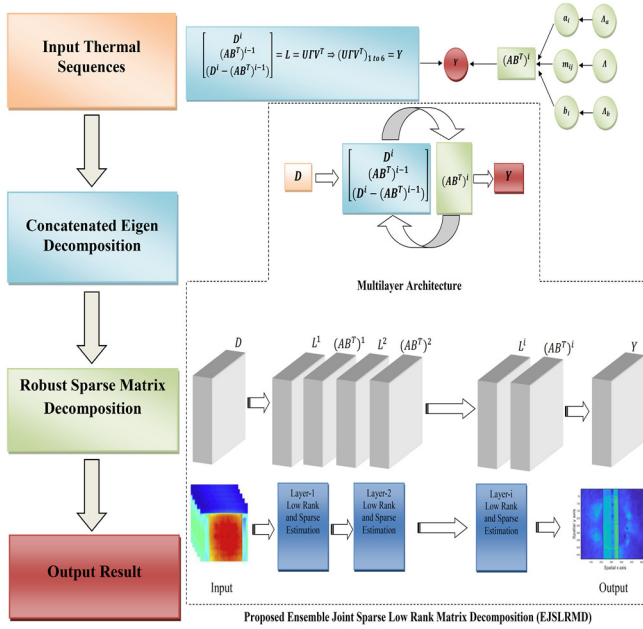
Fig. 1. Proposed model description.

as a vector for i frames. Second, this matrix can be modeled into a multilayer structure [40], [41] of low-rank matrix L, sparse matrix S, and noise matrix E as

$$D^1 = L^1 + S^1 + E^1. \tag{1}$$

For the second layer decomposition, it can be expressed as

$$D^2 = f^1(D^1) + L^2 + S^2 + E^2. \tag{2}$$

In general, for the ith layer, the deep decomposition can be written as

$$D^i = f^{i-1}(D^{i-1}) + L^i + S^i + E^i \tag{3}$$

where $f^i(D^i)$ is the activation used in the multilayer low-rank sparse data modeling. This structure is portrayed in Fig. 1.

Fig. 1 shows the overall schematic block diagram of the proposed model. It is divided into four core parts for better interpretation. The orange blocks represent the input thermal sequences. The blue blocks represent the concatenated feature space eigendecomposition. The green blocks represent the model for the probabilistic robust matrix factorization algorithm. Finally, the red block is the output. Given the input data and initializations of the sparse matrices, the concatenated eigendecomposition is performed as shown in the blue blocks on the top of Fig. 1. In the next step, the sparse matrix decomposition is performed and its probabilistic model is shown by the green block in Fig. 1. This process of EJSLRMD is solved in an iterative manner where the concatenated low-rank component is solved by eigendecomposition and sparse component is solved by an EM approach as shown in the middle blocks of Fig. 1. Finally, the overall process is represented as a multilayer ensemble architecture of the low-rank and sparse factorization as shown in the bottom blocks of Fig. 1. The whole structure is applied to extract the weak defect information on CFRP composites by using optical thermography.

The previous study does not involve or leverage the sparse factors for the spatial resolution of the thermal data. Sparseness refers to a representational scheme where only a few units (out of a large population) are effectively used to represent typical data vectors. In effect, this implies most units taking values close to zero while only few take significantly nonzero values. The sparse factors enforce the solution to consider only the significant region where the defect may lie within the surrounding background. Data with sparse outliers are partially contaminated by noise of overwhelming magnitude, sheer low-rank assumption cannot fully capture its complex structure. Therefore, (1) can be considered as combination of sparse patterns (e.g., hot spots) and nonsparse patterns. Thus, to extract the defect information from the thermographic data, we propose the following optimization problem [44], [45]:

$$\min_{L,S}\left\{\left\|L^i\right\|_* + \Lambda\left\|S^i\right\|_2 + \left\|D^i - L^i - S^i\right\|_F^2\right\} \tag{4}$$

where Λ is the regularizing parameters for S, $\|.\|_2$ represents the l_2 norm, $\|.\|_*$ represents the nuclear norm for low-rank term L, and $\|.\|_F$ represents the Frobenius norm. Using the regularizing framework, we relax the above problem using convex proxies. In addition, for any nonsingular matrix, $S = AS^{-1}SB^T$ holds. The problem (4) can be reformulated as follows:

$$\min_{L,A,B}\left\{\left\|L^i\right\|_* + \Lambda_a\left\|A^i\right\|_2^2 + \Lambda_b\left\|B^i\right\|_2^2 \right.$$
$$\left. + \left\|D^i - L^i - \left(AB^T\right)^i\right\|_F^2\right\} \tag{5}$$

where Λ_a and Λ_b are the regularizing parameters for A and B, respectively. The problem of (5) is solved in two steps. In the first step, we solve for L, which is the low-rank term. In the second step, we solve for $S = AB^i$, which represents the sparse term. The steps are elaborated in graphical form as shown in Fig. 1. For the low-rank term, given the data matrix D and initial matrices A and B, we propose a concatenated eigendecomposition for the low-rank term

$$L^i = \begin{bmatrix} D^i \\ D^i - \left(AB^T\right)^{i-1} \\ \left(AB^T\right)^{i-1} \end{bmatrix} \tag{6}$$

where i represents the layer number. For the problem of defect detection in the CFRP composite structure by using optical thermography, the thermal video sequences contain multiple frames of the same specimen on different transient responses. Based on the analysis in [41] and [40], the defect information is mostly present in the sparse and low-rank components of the decomposition. By concatenating the original data with residual and sparse data for the eigendecomposition, it is able to extract more information of the defects as compared to the simple eigendecomposition without concatenation, which can be seen in the results of PCA [22], as seen in Fig. 4. In particular, this data go into the sparse decomposition algorithm given in [46], which further removes the noise and modifies the sparse data in an iterative manner. By using the concatenated feature space

in a joint sparse and low-rank decomposition, it significantly enhances the extraction of weak defect information.

By concatenating the sparse data, two benefits can be achieved. First, we keep intact the original raw features in the low-rank estimation. This enforces that the estimated low-rank features do not significantly deviate from the original features. Second, we use the sparse data and residual data for low-rank estimation. It significantly embeds the sparse information into the low-rank space, which subsequently allows the algorithm to extract the target weak defect information from both low-rank space and sparse space in a joint optimization framework by using the concatenated feature space. We solve the problem of (6) by using eigendecomposition technique as follows:

$$L^i = U\Gamma V^T \tag{7}$$

where U and V are the left and right eigenmatrices, respectively, and Γ is the diagonal matrix containing the eigenvalues. The first six principal eigenvectors are chosen to represent the low-rank terms. This setting is based on repeated experimental analysis and it is observed that six eigenvectors can already contain the most useful low-rank information, namely

$$Y^i = \left(U\Gamma V^T\right)_{1\ \text{to}\ 6}. \tag{8}$$

For $S = (AB^T)$, we solve the following optimization problem [46]:

$$\left(AB^T\right)^i = \arg \min_{A,B}$$
$$\times \left\{ \left\|Y^i - \left(AB^T\right)^{i-1}\right\|_F^2 + \Lambda_a \left\|A^{i-1}\right\|_2^2 + \Lambda_b \left\|B^{i-1}\right\|_2^2 \right\}. \tag{9}$$

It should be noted that the most expensive step is sparse modeling. As only six principal eigenvectors are used to represent the low-rank terms, the computational cost will be significantly reduced. We solve the problem of (9) for each layer i by using the probabilistic robust matrix factorization (PRMF) algorithm given in [46]. The algorithm given in [46] utilizes the conditional EM (CEM) algorithm given in [47] to update A and B in an iterative manner. First, we decompose Y containing the concatenation information as the following matrix factorization problem [46]:

$$Y = AB^T + E \tag{10}$$
$$a_{ij}\left|\Lambda_a \sim \aleph \left(a_{ij}\left|0, \Lambda_a^{-1}\right.\right)\right. \tag{11}$$
$$b_{ij}\left|\Lambda_b \sim \aleph \left(b_{ij}\left|0, \Lambda_b^{-1}\right.\right)\right. \tag{12}$$

where E is the noise matrix, a_i be the ith row of A, and b_j be the jth row of B. Assuming noise follows the Laplacian distribution. This implicates

$$p\left(E|\Lambda\right) = \left(\frac{\Lambda}{2}\right)^{mn} \exp\left\{-\Lambda\|E\|_1\right\}. \tag{13}$$

Let A and B be the parameters to be estimated. Λ, Λ_a, and Λ_b are the hyperparameters. The MAP theory and Bayes theorem gives

$$p \propto p\left(Y\left|A, B, \Lambda\right.\right) p\left(A\left|\Lambda_a\right.\right) p\left(B\left|\Lambda_b\right.\right) \tag{14}$$

where

$$\log p\left(A, B\left|Y, \Lambda, \Lambda_a, \Lambda_b\right.\right)$$
$$= -\Lambda\left\|Y - AB^T\right\|_1 - \Lambda_a\|A\|_2^2 - \Lambda_b\|B\|_2^2 + C \tag{15}$$

where C is the constant term. The problem of (15) is the same as minimizing the following problem:

$$\min_{A,B}\left\|Y - AB^T\right\|_1 + \Lambda_a\|A\|_2^2 + \Lambda_b\|B\|_2^2. \tag{16}$$

To solve this problem, a leveled hierarchical form of a Laplacian distribution is used. Let y be the Laplacian random variable, its probability density function can be given as

$$p\left(y\left|a, l^2\right.\right) = \frac{l^2}{2}\exp\left(-l^2\left|y - a\right|\right). \tag{17}$$

The Laplacian distribution can be represented as mixture of Gaussians (MoGs) as follows:

$$L\left(y\left|a, l^2\right.\right) = \int_0^\infty \aleph\left(y\left|a, m\right.\right) \text{Expon}\left(m, l^2\right) dm \tag{18}$$

where $\text{Expon}(m, l^2)$ is the exponential distribution term. To accommodate this, a matrix $M = [m_{ij}] \in \mathbb{R}^{m \times n}$ is used whose each element follows exponential prior. This variable relates the l_1 term to the l_2 term and hence we can have a closed-form solution.

Let a_i be the ith row of A and b_j be the jth row of B. The matrix factorization can be formulated as

$$y_{ij}\left|A, B, M \sim \aleph\left(y_{ij}\left|a_i^T b_j, m_{ij}\right.\right)\right. \tag{19}$$
$$a_{ij}\left|\Lambda_a \sim \aleph\left(a_{ij}\left|0, \Lambda_a^{-1}\right.\right)\right. \tag{20}$$
$$b_{ij}\left|\Lambda_b \sim \aleph\left(b_{ij}\left|0, \Lambda_b^{-1}\right.\right)\right. \tag{21}$$
$$m_{ij}\left|\Lambda \sim \text{Expon}\left(m_{ij}|\Lambda/2\right). \tag{22}$$

To estimate A and B, a CEM algorithm is used [47]. The EM algorithm iterates between two steps, E-step and M-step. For the E-step, the Q-function is solved. Given the initial estimates be $\hat{\theta} = [\hat{A}, \hat{B}]$, namely

$$\mathcal{Q}\left(B\left|\hat{\theta}\right.\right) = E_M\left[\log p\left(B\left|\hat{A}, Y, M\right.\right)\left|Y, \hat{\theta}\right.\right]. \tag{23}$$

Taking log on both sides and ignore the terms that do not relate to Q.

$$\log p\left(Y\left|B, \hat{A}, M\right.\right) + \log p\left(B\right)$$
$$= -\frac{1}{2}\sum_i^m \sum_j^n \left\{m_{ij}^{-1}\left(y - \hat{a}_i^T b_j\right)^2\right\} - \Lambda_b \sum_j^n b_j^T b_j + C. \tag{24}$$

It can be seen that m_{ij}^{-1} obeys an inverse Gamma distribution

$$E\left[m_{ij}^{-1}\left|Y, \hat{A}, \hat{B}\right.\right] = \frac{\sqrt{\Lambda}}{|u_{ij}|} \triangleq \left\langle m_{ij}^{-1}\right\rangle \tag{25}$$

where $u_{ij} = y_{ij} - (ab^T)_{ij}$. Next, in the M-step, the parameter B is updated. This is done by maximizing the Q-function. To achieve this, take the partial derivative of Q-function with respect

TABLE I
PROPOSED EJSLRMD

1. Input Data $D \in R^{m \times n \times k}$
2. Convert the tensor D into matrix form.
3. Initialize the parameters Λ_a, Λ_b as 1 and A, B randomly.
4. For each layer do;
5. Solve for L using the (6) to (7).
6. Solve for A and B using CEM algorithm.
7. E-Step: for A and B $\langle m_{ij}^{-1} \rangle = \frac{\sqrt{\lambda}}{|u_{ij}|}$
8. M-Step:
9. $b_j = \left(\widehat{A}^T \Omega_j \widehat{A} + \Lambda_b I_u \right)^{-1} \widehat{A}^T \Omega_j y_{\cdot j}$
10. $a_i = \left(B^T \Lambda_i \widehat{B} + \Lambda_a I_u \right)^{-1} \widehat{B}^T \Lambda_i y_i$.
11. Check the stopping criteria using (28) or go to step 5.
12. End for
13. Output L, S

The Matlab demo code can be linked: http://faculty.uestc.edu.cn/gaobin/zh_CN/lwcg/153392/list/index.htm

to b_j and set it to zero. The update rule can be set as

$$b_j = \left(\hat{A}^T \Omega_j \hat{A} + \Lambda_b I_u \right)^{-1} \hat{A}^T \Omega_j y_{\cdot j} \qquad (26)$$

where $\Omega_j = \mathrm{diag}(\langle m_{1j}^{-1} \rangle, \ldots, \langle m_{mj}^{-1} \rangle)$ and y is the jth column of Y. Following the same convention, the update formula for a can be found as

$$a_i = \left(B^T \Lambda_i \hat{B} + \Lambda_a I_u \right)^{-1} \hat{B}^T \Lambda_i y_i \qquad (27)$$

where $\Lambda_i = \mathrm{diag}(\langle m_{i1}^{-1} \rangle, \cdots, \langle m_{in}^{-1} \rangle)$ and y_i. is the ith row of Y. As the data Y consist of only six principle eigenvectors, the CEM algorithm based on the experimental analysis updates A and B in only two iterations.

The stopping condition for the proposed EJSLRMD is set as follows:

$$\sum_i \frac{\left(u_{ij}^i - u_{ij}^{i-1} \right)}{u_{ij}^{i-1}} < \epsilon. \qquad (28)$$

The term ϵ represents the tolerance level, which has been selected to be 10^{-6} based on the independent Monte Carlo test. The complete step-by-step description is tabulated in Table I.

III. EXPERIMENTAL SETUP

A. Experiment Set-Up and Specimen Details

In an experimental evaluation, Fig. 2 shows the OPT system with the reflection mode configuration [48]. Halogen lamps are used as the source of excitation with the power of 2 kW. At the back hand, an optical excitation source ITECH-IT6726G is used, which is a $ZY - B$ type source. It comes with an adjustable dc power mechanism, which can go up to 3 kW. The distance between the specimen under test and excitation source is set around 80 cm. The A655sc infrared camera is used to capture the time-series temperature variations of the specimen. The resolution of the camera is 640×480. The thermal sensitivity of the camera is 0.05 °C. In our experiments, we have utilized the sampling frequency of 50 Hz.
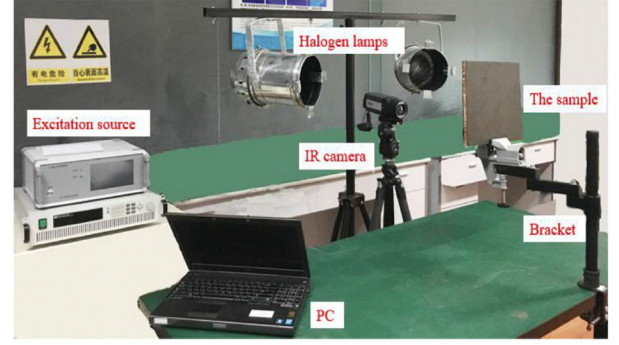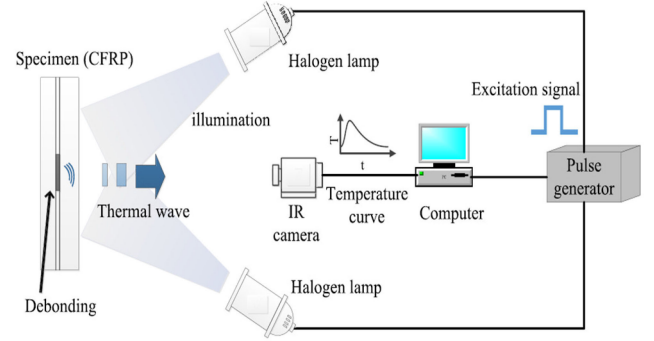

Fig. 2.   OPT system.

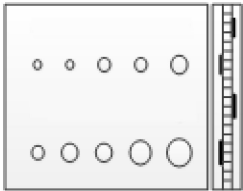Fig. 3.   Block diagram of the OPT system.
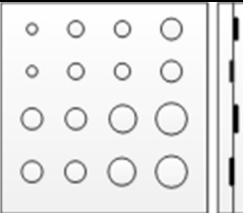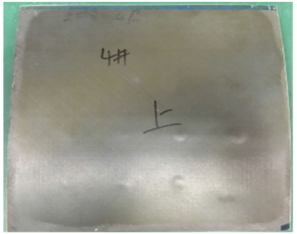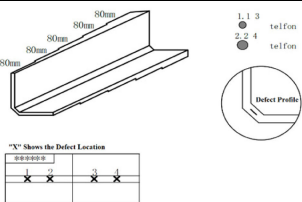
OPT technology utilizes an external heating source and an infrared camera. The specimen is excited using external sources and the temperature variations are captured. These temperature variations are represented as the time series of the thermographic i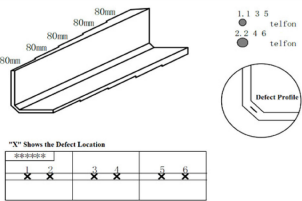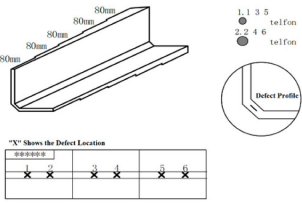mages. The pulse generator is used to control the frequency of excitation and a computer is used to store the results. The configuration of the reflection mode is used with the halogen lamps as the source of heating. The halogen lamps and the infrared camera are placed facing the same direction of the specimen as the reflection mode as shown in the schematic block diagram of OPT in Fig. 3.

Five different CFRP composite specimens are prepared for the experimental validation of the proposed algorithm. The CFRP composites were acquired from the Chengdu Aircraft Design Institute, which is a part of the China Aviation Industry. These specimens were used in the design and manufacturing of the aircraft components. The first two specimens are flat surface with a rectangular shape. The remaining three samples have the V shape irregular surface. All the specimens have debond defects of different diameters and depths. The more detailed information about the specimen and defects can be found in Table II.

IV. EXPERIMENTS ANALYSIS

The visual results along with the quantitative results are presented. The comparative analysis is carried out with the general OPT algorithms to show the efficacy and efficiency of the proposed algorithm. The quantitative comparison

TABLE II
INFORMATION ABOUT THE CFRP SPECIMEN

Number	Defect Profile	Dimension(mm)	Defect Information(mm) Top Depth, Bottom Diameters	Picture
1		250×250×24.2	1, 2 2,4,6,8,10,12,16,20	
2		250×250×22.2	2, 2.5 2,4,6,8	
3		100×100×80	2, 2.25, 2.5,2.75 2, 3	
4		100×100×80	0.5,0.75,1,1.25,1.5,1.75 2, 3	
5		100×100×80	1.5,1.75,2,2.25,2.5,2.75 9, 10	

parameters used are *F*-score and the running (computation) time. The general OPT-based NDT algorithms under comparison are PCA [22], PPT [27], TSR [26], EVBTF [40], and S-MoG [41]. All the experiments are carried out in a corei7 computer with a Windows 10 operating system having 8 GB RAM. MAT-LAB2017b software is utilized for all the algorithms evaluation. The comparative results for all specimens are summarized in Table III.

The visual comparative results are shown in Fig. 4 in a tabular form. Row 1 shows the comparison results for specimen 1. It is a flat surface rectangular shape specimen. The defect depths are 1 mm and 2 mm. For this specimen, almost all the algorithms perform well. However, from Fig. 4 (row 1) left to right, it can be seen that strong noise is still present and all algorithms fail to detect the defect with the smallest diameter defects on the right end corner. Nonetheless, the proposed algorithm gives better

TABLE III
COMPARATIVE RESULTS *F*-SCORE (LEFT) AND TIME TAKEN (RIGHT IN SECONDS)

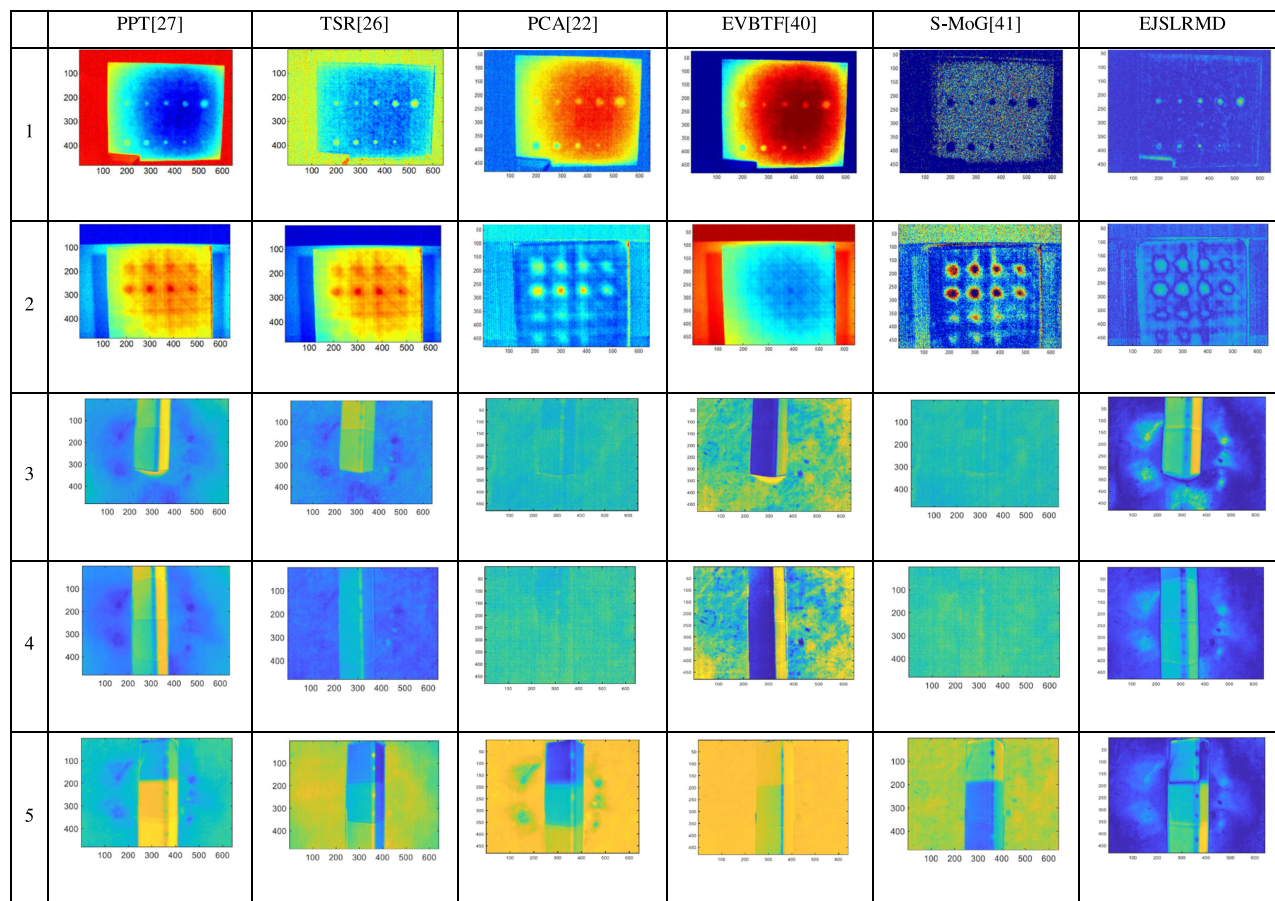| Specimen Number	PPT[27]		TSR[26]		PCA[22]		EVBTF[40]		S-MoG[41]		EJSLRMD	
1	0.94	135	0.94	271	0.94	43	0.94	1342	0.94	173	**1**	51
2	0.66	564	0.66	642	0.93	153	0.30	1019	0.93	466	**0.93**	52
3	0.4	129	0.66	241	0.66	15	0.00	766	0.4	86	**1**	90
4	0.4	124	0.66	631	0.4	30	0.00	1039	0.4	120	**1**	93
5	0.75	146	0.88	601	0.88	47	0.75	753	0.88	125	**1**	95
Average	63%	208	76%	494	76%	56	40%	970	71%	190	**99%**	76

Fig. 4. Comparative analysis of different algorithms.

contrast and resolution result. It detects all the debond defects present on the specimen. Fig. 4 (row 2) shows the results of the second sample with a flat surface and rectangular shape. The defect depths are 2 mm and 2.5 mm. In comparison, the proposed algorithm gives better contrast and resolution and quantifies more defects than the other algorithms.

Fig. 4 (row 3) shows the comparative results for the specimen 3. It is a $V-$ shaped irregular surface specimen. The defect depths are $(2, 2.25, 2.5, 2.75)$ mm. From Fig. 4 (row 3) left to right, most algorithms fail to detect the debond defects. The proposed algorithm is able to give reasonable contrast and resolution results. The proposed algorithm detects all the defects present in the specimen.

Fig. 4 (row 4) shows the visual results for CFRP specimen 4. Here, the number of defects are 6. The depths are $(0.5, 0.75, 1, 1.25, 1.5, 1.75)$ mm. Because of the irregular shape and surface, the performance of these algorithms is quite poor. The proposed algorithm gives better resolution with good contrast results. All the debond defects are successfully detected.

Fig. 4 (row 5) shows the visual results for specimen 5. The number of defects here are 5. The depth of the defects are $(1.5, 1.75, 2, 2.25, 2.5)$ mm. The diameter of the defects are 9 mm and 10 mm. In the comparative analysis, the proposed algorithm detects all the debond defects present on the specimen and shows good resolution and contrast.

The quantitative comparison based on *F*-score and computation time is tabulated in Table III. The last row shows the average percent *F*-score for all the algorithms along with the average computation time in seconds. On average, the PPT algorithm has the detection efficiency of 63% with 208 s in average running time. The average detection rate in terms of percent *F*-score for the TSR algorithm is 76% with the average time consumption of 494 s. The PCA algorithm has the fastest running time of 56 s with a reasonable detection rate of 76%. The algorithm of EVBTF gives the highest running time of 970 s with a poor detection capability of 40%. The S-MoG algorithm takes an average time of 190 s to produce the results with the percent efficiency of 71%. The proposed algorithm gives on average the highest detection rate of 99%. The proposed algorithm takes around on average 76 s to be the second-fastest algorithm to PCA. By jointly optimizing the low-rank and sparse data in a concatenated manner, it can remove the noise, improve the resolution, and increase the detection efficiency.

The proposed model uses the PRMF [46] algorithm for the sparse decomposition step. However, there are other similar algorithms in the literature. In [49], Xiong *et al.* proposed a matrix factorization algorithm called direct robust matrix factorization algorithm. The block coordinate descent approach is proposed to solve the low-rank decomposition problem, which is a variation of the SVD and efficient thresholding. In [50], Wang and Yeung proposed a Bayesian extension to the PRMF [46] model for the image and video processing applications. In [51], Zhao *et al.* proposed a model for the LRMF problem, which utilizes the inference-based variational Bayes framework. It has been found that these classes of algorithms have high computational cost for the problem of defect detection in CFRP composites. In [52], Meng and Torre proposed a novel model for the LRMF problem, where they assume the noise to have an unknown probabilistic distribution and estimate it by using an MoG model. In [53], Cao *et al.* improved the model given in [52] by assuming that the noise has mixture of exponential power (MoEP) distribution and propose an EM algorithm to solve the problem. In [54], Kim and Oh proposed a novel algorithm for the LRMF problem, which utilizes the orthogonal matrix decomposition algorithm in the augmented Lagrangian framework. In [55], Lin *et al.* proposed a majorization–minimization approach for the problem of LRMF. A surrogate function is used to replace the original problem and the algorithm of a linearized alternating direction method with parallel splitting and adaptive penalty is used for its solution owing to its low computation cost.

The algorithm given in [49] is a simple and an easy way to implement, whereas its performance is normal. The algorithms given in [50] and [51] are based on the Bayesian framework. The class of variational Bayes framework based algorithms for the problem of defect detection in CFRP composites using optical thermography have been analyzed by Lu *et al.* [40]. These algorithms have poor performance and high computation cost for an irregular shape CFRP specimen. The algorithms given in [52]–[55] are quite robust and assume that the noise has a more complex distribution rather than the Gaussian distribution. These classes of algorithms were analyzed in [41]. It has been found that these algorithms for the defect detection problem with
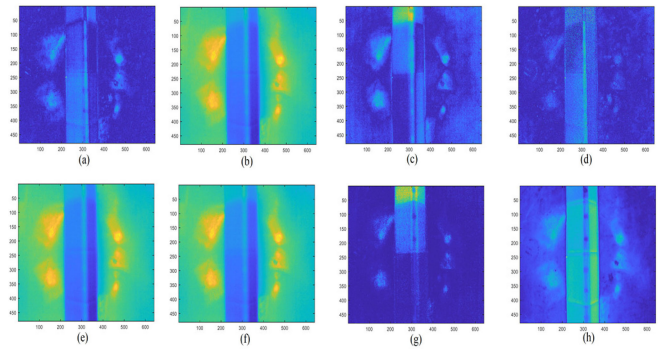

Fig. 5. Comparative results for specimen 4 on different algorithms and their computation time in seconds. (a) [52] (156 s). (b) [50] (1986 s). (c) [53] (340 s). (d) [55] (420 s). (e) [42] (464 s). (f) [35] (29 s). (g) [38] (14 s). (h) proposed (93 s).

the irregular shape specimen fail to perform well. In addition, these algorithms are quite complex and lots of parameters need to be tuned for the solution of a particular problem. Based on this analysis, the PRMF [46] algorithm was selected owing to its simple implementation, less parameter tuning, and robustness to fit in the framework of EJSLRMD. In the multilayer architecture of EJSLRMD, it requires more parameters and complex architecture, which increases the computational cost as referred in [40] and [41]. The PRMF algorithm in the proposed framework converges significantly fast and simultaneously it is able to recover the signal more accurately with complex noise distributions.

Fig. 5 shows the comparative results on specimen 4 with irregular shape that has six defects on varying depths. Fig. 5(a) shows the results of the matrix factorization algorithm given in [52]. It can be observed from the results that it is difficult to distinguish the defects and background. The computational cost is 156 s. Fig. 5(b) is the result of Bayesian robust matrix factorization algorithm given in [50]. The results are over smooth and defects are not clearly visible. The computational cost is significant high of 1986 s. Fig. 5(c) shows the result of exponential power distribution based algorithm [53]. Here the noise is assumed to have a more complex distribution. However, the algorithm is unable to detect the defects clearly. The computational cost of this algorithm is 340 s. Fig. 5(d) shows the result of matrix factorization algorithm in [55]. However, it is unable to detect the defects and its computational time is 420 s. Fig. 5(e) shows the result of tridecomposition model given in [42] called the stable principal component pursuit. The computational cost is 464 s. The result is over smooth and defects are hidden in the background and blurry. Fig. 5(f) shows the results of a state-of-the-art algorithm given in [35] called the SPCT. The computational time is very less 29 s. However, as the CFRP specimen has an irregular shape and varying depth, the algorithm is unable to detect the defect more clearly. Fig. 5(g) shows the results of a nonnegative matrix factorization algorithm given in [38]. This algorithm has least computational cost of 14 s. The algorithm is able to detect at most three defects out of six with a strong noise present. The last figure shows the result of the proposed algorithm. The computational time is 93 s. It can be seen that

TABLE IV
EXPERIMENTAL ANALYSIS ON SYNTHETIC DATA WITH DIFFERENT NOISE CONFIGURATIONS

| Rank(10)		PCA[22]	RPCA[56]	BRPCA[57]	VBRPCA[58]	PRMF[46]	MoG[59]	S-MoG[41]	Proposed
No Noise	RRE	**1.80e-15**	1.76e-8	0.196	1.18e-3	1.56e-5	1.52e-4	2.33e-6	1.98e-8
	Time(s)	**0.0019**	0.0961	46.61	0.0190	0.342	0.160	0.280	0.190
Sparse Noise	RRE	0.789	3.39e-3	7.99e-2	0.863	7.11e-5	8.44e-5	6.60e-6	**7.48e-7**
	Time(s)	**0.0041**	0.187	40.11	0.116	0.710	0.310	0.417	0.380
Gaussian Noise	RRE	3.10e-2	5.10e-2	3.19e-2	4.96e-2	3.91e-2	3.14e-2	1.16e-3	**6.48e-4**
	Time(s)	**0.0037**	0.179	88.69	0.120	0.640	0.310	0.569	0.480
Mixture Noise	RRE(s)	1.07	0.109	7.66e-2	1	7.44e-2	2.64e-2	4.56e-3	**9.04e-3**
	Time	**0.0036**	0.180	28.66	0.862	0.622	1.36	1.98	1.56
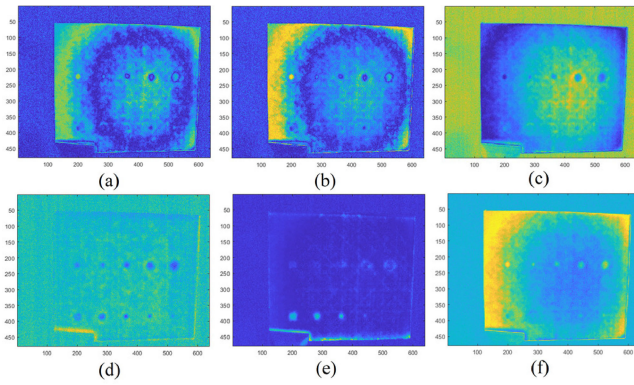
Fig. 6. Inherent layering results for the specimen 1. (a) Layer 1. (b) Layer 2. (c) Layer 3. (d) Layer 4. (e) Layer 5. (f) Layer 6.

the proposed algorithm is able to detect all defects clearly with good resolution and reasonable computational cost. For the case of debond detection in CFRP composites with irregular shape and varying depth, the proposed EJSLRMD algorithm provides better quality and detection results under comparison with recent matrix factorization and other infrared nondestructive testing state-of-the-art algorithms.

The proposed algorithm is tested on the synthetic data for modeling different types of noise and results as presented in Table IV. A series of matrix decomposition based algorithms are compared. The results are quoted in terms of the relative reconstruction error (RRE) and time in seconds. Table IV shows that the proposed algorithm is able to recover the mixture of noise more accurately as compared with the other algorithms of PCA [22], robust PCA (RPCA) [56], Bayesian RPCA (BRPCA) [57], variational Bayesian PCA (VBRPCA) [58], PRMF [46], MoG [59], and S-MoG [41]. The best results are highlighted in bold. It can be seen that the proposed algorithm is able to recover the signal with least error when the noise is considered as the complex noise also the time taken is reasonable as compared with other algorithms.

Fig. 6 shows the inherent layering results for specimen 1. The proposed algorithm is able to detect and quantify the defects up to layer 4 for this specimen. Further layering induces overfitting of the data and the results get worse as can be seen from Fig. 6(e) and (f).

V. CONCLUSION

In this article, a joint low-rank sparse modeling algorithm was proposed. The algorithm was evaluated for inner debond defects

as well as on synthetic data for modeling the complex noise. By optimizing the low-rank and sparse data using the concatenated feature space helped to boost the computation speed, estimate the complex noise, and detect weaker information defects hidden in the background. The quantitative results based on *F*-score and RRE proved that the proposed model performed well in modeling complex noise and quantifying weaker debond defects presented on the irregular shape CFRP composites. The comparative analysis with general OPTNDT and low-rank sparse modeling algorithms proved the efficacy of the proposed model.

In future works, the proposed model will be validated on more challenging CFRP specimen with irregular shape and varying depth. The proposed method will be applied across wider infrared measurement technology such as eddy current pulsed thermography. The computational complexity of the model will be further improved for online NDT.

REFERENCES

[1] H. Fernandes, H. Zhang, A. Figueiredo, C. Ibarra-Castanedo, G. Guimarares, and X. Maldague, "Carbon fiber composite inspection and defect characterization using active infrared thermography: numerical simulations and experimental results," *Appl. Opt.*, vol. 55, no. 34, pp. 46–53, 2016.

[2] C. Maierhofer, P. Myrach, M. Reischel, H. Steinfurth, M. Röllig, and M. Kunert, "Characterizing damage in CFRP structures using flash thermography in reflection and transmission configurations," *Compos. B Eng.*, vol. 57, pp. 35–46, 2014.

[3] A. Poudel, K. R. Mitchell, T. P. Chu, S. Neidigk, and C. Jacques, "Nondestructive evaluation of composite repairs by using infrared thermography," *J. Compos. Mater.*, vol. 50, no. 3, pp. 351–363, 2016.

[4] C. Meola, S. Boccardi, G. M. Carlomagno, N. D. Boffa, E. Monaco, and F. Ricci, "Nondestructive evaluation of carbon fibre reinforced composites with infrared thermography and ultrasonics," *Compos. Struct.*, vol. 134, pp. 845–853, 2015.

[5] B. Gao, W. L. Woo, Y. He, and G. Y. Tian, "Unsupervised sparse pattern diagnostic of defects with inductive thermography imaging system," *IEEE Trans. Ind. Informat.*, vol. 12, no. 1, pp. 371–383, Feb. 2016.

[6] D. Palumbo, R. Tamborrino, U. Galietti, P. Aversa, A. Tatì, and V. A. M. Luprano, "Ultrasonic analysis and lock-in thermography for debonding evaluation of composite adhesive joints," *NDT E Int.*, vol. 78, pp. 1–9, 2016.

[7] V. Munoz *et al.*, "Damage detection in CFRP by coupling acoustic emission and infrared thermography," *Compos. B Eng.*, vol. 85, pp. 68–75, 2016.

[8] B. Gao, W. L. Woo, G. Y. Tian, and H. Zhang, "Unsupervised diagnostic and monitoring of defects using waveguide imaging with adaptive sparse representation," *IEEE Trans. Ind. Informat.*, vol. 12, no. 1, pp. 405–416, Feb. 2016.

[9] Z. Wang, G. Tian, M. Meo, and F. Ciampa, "Image processing based quantitative damage evaluation in composites with long pulse thermography," *NDT E Int.*, vol. 99, pp. 93–104, 2018.

[10] H. Zhang *et al.*, "An infrared-induced terahertz imaging modality for foreign insert detection in a glass fiber-skinned lightweight honeycomb composite panel," *IEEE Trans. Ind. Informat.*, vol. 14, no. 12, pp. 5629–5636, Dec. 2018.

[11] H. Zhang *et al.*, "Optical excitation thermography for twill/plain weaves and stitched fabric dry carbon fibre preform inspection," *Composites A Appl. Sci. Manuf.*, vol. 107, pp. 282–293, 2018.

[12] H. Zhang *et al.*, "Optical and mechanical excitation thermography for impact response in basalt-carbon hybrid fiber-reinforced composite laminates," *IEEE Trans. Ind. Informat.*, vol. 14, no. 2, pp. 514–522, Feb. 2018.

[13] V. P. Vavilov, "Modeling and characterizing impact damage in carbon fiber composites by thermal/infrared non-destructive testing," *Compos. B Eng.*, vol. 61, pp. 1–10, 2014.

[14] R. Yang and Y. He, "Optically and non-optically excited thermography for composites: A review," *Infrared Phys. Technol.*, vol. 75, pp. 26–50, 2016.

[15] C. H. Ryu, S. H. Park, D. H. Kim, K. Y. Jhang, and H. S. Kim, "Nondestructive evaluation of hidden multi-delamination in a glass-fiber-reinforced plastic composite using terahertz spectroscopy," *Compos. Struct.*, vol. 156, pp. 338–347, 2016.

[16] A. O. Chulkov and V. P. Vavilov, "Hardware and software for thermal nondestructive testing of metallic and composite materials," in *Proc. J. Phys. Conf. Ser.*, 2016, vol. 671, no. 1, pp. 1–6.

[17] X. Bai, Y. Fang, W. Lin, L. Wang, and B. F. Ju, "Saliency-based defect detection in industrial images by using phase spectrum," *IEEE Trans. Ind. Informat.*, vol. 10, no. 4, pp. 2135–2145, Nov. 2014.

[18] G. Acciani, G. Brunetti, and G. Fornarelli, "Application of neural networks in optical inspection and classification of solder joints in surface mount technology," *IEEE Trans. Ind. Informat.*, vol. 2, no. 3, pp. 200–209, Aug. 2006.

[19] D. M. Tsai, I. Y. Chiang, and Y. H. Tsai, "A shift-tolerant dissimilarity measure for surface defect detection," *IEEE Trans. Ind. Informat.*, vol. 8, no. 1, pp. 128–137, Feb. 2012.

[20] W. C. Li and D. M. Tsai, "Defect inspection in low-contrast LCD images using hough transform-based nonstationary line detection," *IEEE Trans. Ind. Informat.*, vol. 7, no. 1, pp. 136–147, Feb. 2011.

[21] A. Picon, O. Ghita, P. F. Whelan, and P. M. Iriondo, "Fuzzy spectral and spatial feature integration for classification of nonferrous materials in hyperspectral data," *IEEE Trans. Ind. Informat.*, vol. 5, no. 4, pp. 483–494, Nov. 2009.

[22] N. Rajic, "Principal component thermography for flaw contrast enhancement and flaw depth characterisation in composite structures," *Composite Struct.*, vol. 58, no. 4, pp. 521–528, 2002.

[23] H.-C. Kim, D. Kim, and S. Y. Bang, "An efficient model order selection for PCA mixture model," *Pattern Recognit. Lett.*, vol. 24, no. 9, pp. 1385–1393, 2003.

[24] S. Marinetti *et al.*, "Statistical analysis of IR thermographic sequences by PCA," *Infrared Phys. Technol.*, vol. 46, pp. 85–91, 2004.

[25] A. Hyvärinen and E. Oja, "Independent component analysis: Algorithms and applications," *Neural Netw.*, vol. 13, no. 4/5, pp. 411–430, 2000.

[26] S. M. Shepard and M. Frendberg Beemer, "Advances in thermographic signal reconstruction," *Proc. SPIE*, vol. 9485, pp. 1–7, 2015.

[27] X. Maldague and S. Marinetti, "Pulse phase infrared thermography," *J. Appl. Phys.*, vol. 79, no. 5, pp. 2694–2698, 1996.

[28] C. Ibarra-Castanedo and X. Maldague, "Pulsed phase thermography reviewed," *Quant. Infrared Thermogr. J.*, vol. 1, no. 1, pp. 47–70, 2004.

[29] L. Yuanlin, T. Qingju, B. Chiwu, M. Chen, W. Pingshan, and Z. Jiansuo, "Pulsed infrared thermography processing and defects edge detection using FCA and ACA," *Infrared Phys. Technol.*, vol. 72, pp. 90–94, 2015.

[30] B. Yousefi, S. Sfarra, C. Ibarra-Castanedo, and X. P. V. Maldague, "Comparative analysis on thermal non-destructive testing imagery applying candid covariance-free incremental principal component thermography (CCIPCT)," *Infrared Phys. Technol.*, vol. 85, pp. 163–169, 2017.

[31] F. López, V. P. Nicolau, C. Ibarra-Castanedo, S. Sfarra, and X. Maldague, "Comparative study of thermographic signal reconstruction and partial least squares thermography for the detection and evaluation of subsurface defects flash-lamps," in *Proc. Int. Conf. Quant. Infrared Thermogr.*, 2014, pp. 1–10.

[32] L. Junyan, W. Fei, L. Yang, and W. Yang, "Inverse methodology for identification the thermal diffusivity and subsurface defect of CFRP composite by lock-in thermographic phase (LITP) profile reconstruction," *Compos. Struct.*, vol. 138, pp. 214–226, 2016.

[33] L. Zhang, Q. Zhang, L. Zhang, D. Tao, X. Huang, and B. Du, "Ensemble manifold regularized sparse low-rank approximation for multiview feature embedding," *Pattern Recognit.*, vol. 48, no. 10, pp. 3102–3112, 2015.

[34] M. Ishikawa *et al.*, "Reducing inspection time of pulse phase thermography by using phase data at higher frequency range," *Infrared Phys. Technol.*, vol. 92, pp. 53–59, 2018.

[35] B. Yousefi, S. Sfarra, F. Sarasini, and X. P. V. Maldague, "IRNDT inspection via sparse principal component thermography," in *Proc. Can. Conf. Elect. Comput. Eng.*, 2018, pp. 1–4.

[36] J. Y. Wu, S. Sfarra, and Y. Yao, "Sparse principal component thermography for subsurface defect detection in composite products," *IEEE Trans. Ind. Informat.*, vol. 14, no. 12, pp. 5594–5600, Dec. 2018.

[37] S. Marinetti, L. Finesso, and E. Marsilio, "Matrix factorization methods: Application to thermal NDT/E," *NDT E Int.*, vol. 39, no. 8, pp. 611–616, 2006.

[38] B. Yousefi, S. Sfarra, C. Ibarra-Castanedo, N. P. Avdelidis, and X. P. V. Maldague, "Thermography data fusion and nonnegative matrix factorization for the evaluation of cultural heritage objects and buildings," *J. Therm. Anal. Calorimetry*, vol. 136, no. 2, pp. 943–955, 2018.

[39] Q. Feng *et al.*, "Automatic seeded region growing for thermography debonding detection of CFRP," *NDT E Int.*, vol. 99, pp. 36–49, 2018.

[40] P. Lu, B. Gao, Q. Feng, Y. Yang, W. L. Woo, and G. Y. Tian, "Ensemble variational Bayes tensor factorization for super resolution of CFRP debond detection," *Infrared Phys. Technol.*, vol. 85, pp. 335–346, 2017.

[41] J. Ahmed, B. Gao, G. Y. Tian, Y. Yang, and Y. C. Fan, "Sparse ensemble matrix factorization for debond detection in CFRP composites using optical thermography," *Infrared Phys. Technol.*, vol. 92, pp. 392–401, 2018.

[42] Z. Zhou, X. Li, J. Wright, E. Candès, and Y. Ma, "Stable principal component pursuit," in *Proc. IEEE Int. Symp. Inf. Theory*, 2010, pp. 1518–1522.

[43] A. Aravkin, S. Becker, V. Cevher, and P. Olsen, "A variational approach to stable principal component pursuit," in *Proc. 13th Conf. Uncertainty Artif. Intell.*, 2014, pp. 32–41.

[44] O. Oreifej, X. Li, and M. Shah, "Simultaneous video stabilization and moving object detection in turbulence," *IEEE Trans. Pattern Anal. Mach. Intell.*, vol. 35, no. 2, pp. 450–452, Feb. 2013.

[45] F. Zhang, M. Jin, and F. Chen, "Tri-decomposition model for image recovery," *Electron. Lett.*, vol. 54, no. 23, pp. 163–173, 2018.

[46] N. Wang, T. Yao, J. Wang, and D.-Y. Yeung, "A probabilistic approach to robust matrix factorization," in *Proc. Eur. Conf. Comput. Vision*, 2012, vol. 7578, pp. 126–139.

[47] T. Jebara and A. Pentland, "Maximum conditional likelihood via bound maximization and the CEM Algorithm," in *Proc. Adv. Neural Inf. Process. Syst.*, 1998, pp. 494–500.

[48] Y. He, R. Yang, H. Zhang, D. Zhou, and G. Wang, "Volume or inside heating thermography using electromagnetic excitation for advanced composite materials," *Int. J. Thermal Sci.*, vol. 111, pp. 41–49, 2017.

[49] L. Xiong, X. Chen, and J. Schneider, "Direct robust matrix factorization for anomaly detection," in *Proc. IEEE Int. Conf. Data Mining*, 2011, pp. 844–853.

[50] N. Wang and D. Y. Yeung, "Bayesian robust matrix factorization for image and video processing," in *Proc. IEEE Int. Conf. Comput. Vision*, 2013, pp. 1785–1792.

[51] Q. Zhao, D. Meng, Z. Xu, W. Zuo, and Y. Yan, "L_1-norm low-rank matrix factorization by variational bayesian method," *IEEE Trans. Neural Netw. Learn. Syst.*, vol. 26, no. 4, pp. 825–839, Apr. 2015.

[52] D. Meng and F. D. L. Torre, "Robust matrix factorization with unknown noise," in *Proc. IEEE Int. Conf. Comput. Vision*, 2013, pp. 1337–1344.

[53] X. Cao *et al.*, "Low-rank matrix factorization under general mixture noise distributions," in *Proc. IEEE Int. Conf. Comput. Vision*, 2015, pp. 1493–1501.

[54] E. Kim and S. Oh, "Robust orthogonal matrix factorization for efficient subspace learning," *Neurocomputing*, vol. 167, pp. 218–229, 2015.

[55] Z. Lin, C. Xu, and H. Zha, "Robust matrix factorization by majorization minimization," *IEEE Trans. Pattern Anal. Mach. Intell.*, vol. 40, no. 1, pp. 208–220, Jan. 2018.

[56] J. Wright, Y. Peng, Y. Ma, A. Ganesh, and S. Rao, "Robust principal component analysis: Exact recovery of corrupted low-rank matrices," in *Proc. Adv. Neural Inf. Process. Syst.*, 2009, pp. 2080–2088.

[57] X. Ding, L. He, and L. Carin, "Bayesian robust principal component analysis," *IEEE Trans. Image Process.*, vol. 20, no. 12, pp. 3419–3430, Dec. 2011.

[58] S. D. Babacan, M. Luessi, R. Molina, and A. K. Katsaggelos, "Sparse bayesian methods for low-rank matrix estimation," *IEEE Trans. Signal Process.*, vol. 60, no. 8, pp. 3964–3977, Aug. 2012.

[59] H. Yong, D. Meng, W. Zuo, and L. Zhang, "Robust online matrix factorization for dynamic background subtraction," *IEEE Trans. Pattern Anal. Mach. Intell.*, vol. 40, no. 7, pp. 1726–1740, Jul. 2018.

Junaid Ahmed received the B.E. degree in telecommunications engineering from Mehran University of Engineering and Technology, Jamshoro, Pakistan, in 2010, and the M.S. degree in electrical and electronics engineering from Eastern Mediterranean University, North Cyprus, Turkey, in 2015. He is currently working toward the Ph.D. degree in nondestructive testing and structural health monitoring using infrared thermography with the University of Electronic Science and Technology of China, Chengdu, China.

He is currently an Assistant Professor with Sukkur IBA University, Sukkur, Pakistan. His current research interests include wavelet processing, debond damage, quantitative nondestructive testing and evaluation, sparse representations, and low-rank matrix/tensor factorization.

Bin Gao (Senior Member, IEEE) received the B.Sc. degree in communications and signal processing from Southwest Jiao Tong University, Chengdu, China, in 2005, and the M.Sc. (with distinction) degree in communications and signal processing and the Ph.D. degree in signal processing from Newcastle University, Newcastle upon Tyne, U.K., in 2007 and 2011, respectively.

From 2011–2013, he was a Research Associate with Newcastle University on wearable acoustic sensor technology. He is a currently a Professor with the School of Automation Engineering, University of Electronic Science and Technology of China, Chengdu, China. His current research interests include electromagnetic and thermography sensing, machine learning, and nondestructive testing and evaluation and he actively authored or coauthored in these areas.

Dr. Gao is also a very active Reviewer for many international journals and long-standing conferences. He has coordinated several research projects from National Natural Science Foundation of China.

Wai Lok Woo (Senior Member, IEEE) received the B.Eng. degree in electrical and electronics engineering and the M.Sc. and Ph.D. degrees in machine learning from Newcastle University, Newcastle upon Tyne, U.K., in 1993, 1995, and 1998, respectively.

He was the Director of Research for the Newcastle Research and Innovation Institute and the Director of Operations for Newcastle University. He is currently a Professor of Machine Learning with Northumbria University, Newcastle upon Tyne, U.K. He has authored or coauthored more than 350 papers on these topics on various journals and international conference proceedings. His current research interests include the mathematical theory and algorithms for data science and analytics, artificial intelligence, machine learning, data mining, latent component analysis, multidimensional signal, and image processing.

Dr. Woo is a member of the Institution Engineering Technology. He is an Associate Editor to several international signal processing journals, including the *IET Signal Processing*, *Journal of Computers*, and *Journal of Electrical and Computer Engineering*. He was a recipient of the IEE Prize and the British Commonwealth Scholarship.

Yuyu Zhu received the B.S. degree in automation and the M.Sc. degree in control theory and control engineering from the University of Science and Technology, Hefei, China, in 2002 and 2009, respectively, and is currently working toward the Ph.D. degree in electromagnetic nondestructive testing with the University of Electronic Science and Technology of China, Chengdu, China.

He is currently an Associate Professor on monitoring and control technology and power electronics technology with the School of Automation Engineering. His current research interests include nondestructive testing and evaluation and power electronics technology.